

See discussions, stats, and author profiles for this publication at: <https://www.researchgate.net/publication/216610842>

# Shish Formation and Relaxation in Sheared Isotactic Polypropylene Containing Nucleating Particles

ARTICLE in MACROMOLECULES · MAY 2011

Impact Factor: 5.8 · DOI: 10.1021/ma200040s

---

CITATIONS

43

---

READS

35

## 4 AUTHORS, INCLUDING:



Andrew William Phillips

20 PUBLICATIONS 236 CITATIONS

[SEE PROFILE](#)



Amita Bhatia

Monash University (Australia)

8 PUBLICATIONS 154 CITATIONS

[SEE PROFILE](#)



Graham Edward

Monash University (Australia)

30 PUBLICATIONS 514 CITATIONS

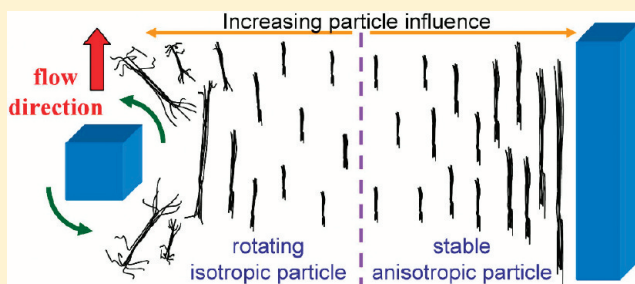
[SEE PROFILE](#)

## Shish Formation and Relaxation in Sheared Isotactic Polypropylene Containing Nucleating Particles

Andrew W. Phillips,\* Amita Bhatia, Peng-wei Zhu, and Graham Edward

Department of Materials Engineering, Co-operative Research Centre for Polymers, Monash University, Clayton VIC 3800, Australia

**ABSTRACT:** The formation and relaxation of shish in molten isotactic polypropylene (iPP) and two samples containing different commercial nucleating particles was studied during and after continuous shear flow. In-situ measurements of the shish were made by simultaneous wide- and small-angle X-ray scattering (rheo-SAXS/WAXS) using synchrotron radiation. In the SAXS patterns, sharp meridional reflections were observed in all three samples during the initial stages of shear flow. Their presence indicates that shish form in discrete steps, by the aggregation of pointlike nuclei into oriented threads. Compared to pure iPP, the addition of both nucleants increased the amount and the dimensions of shish formed. However, the shish also relaxed faster in the presence of both nucleated materials. This behavior was attributed to the particles inducing lower molecular weight chains to participate in shish formation. The particle aspect ratio was observed to greatly influence shish formation. This is explained by modification of the local strain environment near the surface of the different shaped particles.



### 1. INTRODUCTION

Thermoplastic polyolefins such as isotactic polypropylene (iPP) and polyethylene (PE) are typically processed into their final forms by injection molding or extrusion technologies. If the flow intensity in these processes is sufficient, a highly anisotropic crystalline architecture termed shish-kebabs can form,<sup>1–8</sup> which can substantially influence the final physical properties of the component.<sup>9,10</sup> A highly oriented threadlike core composed of extended chains (shish) is considered to form first, which then provides a template for the formation and growth of oriented chain-folded lamellae (kebabs). Accordingly, the formation of shish is one of the key components to understanding morphology development under flow conditions.

For a given polymer, a critical flow intensity is necessary to form shish. However, the specific flow conditions responsible for this transition have only recently been identified.<sup>3,4</sup> The shear rate needs to be larger than the inverse Rouse time of the longest chains (i.e.,  $\dot{\gamma} > 1/t_r$ ) such that the chains can become extended by the flow. Furthermore, a critical amount of mechanical work is also necessary to allow the extended chains to come together and form a stable shish entity. Although the specific flow conditions for shish formation have been identified, the mechanism responsible for the initial shish formation is still under debate.<sup>1,5,6,11–22</sup>

Recent advances in wide- and small-angle X-ray scattering (WAXS/SAXS) techniques have allowed shish formation and relaxation to be probed in situ after controlled shear treatments. Balzano et al.<sup>23</sup> investigated a high-density polyethylene (HDPE), which had been specially prepared to have a bimodal molecular weight distribution, and found shish were able to be formed near to and even slightly above the equilibrium melting temperature of the unconstrained extended chain crystal. It was considered

that to form the shish required the stretch of the longest chains in the molecular weight distribution. A similar conclusion was drawn by Keum et al.,<sup>24</sup> who investigated shish formation and relaxation in model blends of ultrahigh molecular weight polyethylene (UHMWPE) in HDPE. In addition, Keum et al. showed that shish could grow by an autocatalytic process after the shear flow had stopped. Similar autocatalytic growth of shish was also recently observed by Patil et al.<sup>25</sup> in a broad molecular weight PE. Nevertheless, comparable studies have yet to be performed for other commercially important semicrystalline polymers such as iPP.

The crystallization of polymers is complicated by the inclusion of a wide range of particulate additives in polymer formulations such as nucleating agents, colorants, and reinforcing agents. Under quiescent conditions (i.e., without concurrent deformation) these heterogeneous particles can act as nucleation sites, enhancing crystal nucleation and thereby influencing crystallization kinetics and the final morphology of the polymer. The number of active heterogeneous nucleation sites is strongly related to factors that influence the particle surface area available for nucleation. The most common factors affecting this are the concentration and dispersion of particles in the polymer matrix. Yet many other particle characteristics have also been implicated in influencing the nucleation of polymers under quiescent conditions such as epitaxy,<sup>26,27</sup> particle size,<sup>28</sup> particle curvature,<sup>29,30</sup> and porosity.<sup>31</sup>

Foreign particles can also dramatically alter the crystallization kinetics and the development of morphology under flow conditions.

**Received:** January 8, 2011

**Revised:** February 27, 2011

**Published:** April 14, 2011

The combined effects of shear and the addition of particles have been suggested to yield a synergistic increase in the number of active nuclei, raising crystallization rates further than their individual contribution.<sup>32–37</sup> Furthermore, the addition of particles has been shown to decrease the shear intensity required to form the shish-kebab structure.<sup>15,16,25,28,35,38–43</sup> A number of particle characteristics have also been suggested to influence the formation of shear-induced nuclei. Zhu and coauthors<sup>40,41</sup> suggested the surface curvature of the particles may influence the stability of shish forming on the surface of the particle. D'Haese et al.<sup>28</sup> investigated the influence of particle size under a wide range of shear rates and found that the critical shear rate for shish formation decreased with increasing particle size. However, the influence of the nucleation efficiency of the particles, which also increased with particle size, could not be entirely ruled out. Recently, Patil et al.<sup>25</sup> observed that single wall carbon nanotubes (SWCNT) led to increased shish formation, while zirconia nanoparticles destabilized shish formation. Patil explained this by the stronger chain–particle interaction of the SWCNT retarding the relaxation of extended chains compared to the weaker chain–particle interactions of the zirconia nanoparticles. Byelov et al.<sup>36</sup> showed that the shape of the particle could influence the number of shear-induced nuclei, with anisotropic particles leading to greater numbers of shear-induced nuclei compared to isotropic particles. However, the mechanism responsible for this interesting influence of particle shape was not able to be identified.

In this study, continuous shear flow was applied to the melt of pure iPP and melts of two iPP samples containing different commercial nucleating particles. The shear temperature ( $T_\gamma = 181^\circ\text{C}$ ) was selected to be well above the lamellar melting point ( $T_m = 166^\circ\text{C}$ ) of the polymer but below the equilibrium melting temperature of the unconstrained extended chain crystal ( $T_m^0(\text{iPP}) = 186.1^\circ\text{C}$ <sup>44</sup>). The purpose was to investigate the influence of the two nucleating particles on (a) the formation of shish under close to steady-state shear conditions and (b) the shish stability after shear flow was stopped. The likely mechanisms of shish formation and the influence of nucleating particles on shish formation are discussed.

## 2. EXPERIMENTAL SECTION

**2.1. Materials.** The polymer used was an iPP homopolymer manufactured by Borealis (HD601CF). This grade was chosen as it has been extensively investigated by our group and was selected due to its low intentional additive profile. In particular, it contained no calcium stearate, which has previously been shown to induce a high-temperature smectic phase.<sup>45</sup> The average weight molecular weight ( $M_w$ ) and the average number molecular weight ( $M_n$ ) were 367 000 and 74 000 g/mol, respectively. The lamellar melting point of the polymer was determined to be 166 °C using differential scanning calorimetry (DSC).

Two common commercial nucleating particles which specifically nucleate the alpha phase of iPP ( $\alpha$ -iPP) were used in this study: sodium benzoate (SB) and bicyclo[2.2.1]heptane-2,3-dicarboxylic acid, trade name HPN-68 (HPN). Various loadings of the two particles were compounded into the molten iPP at 175 °C in a Haake Rheocord 90 batch mixer and mixed at 60 rpm for 300 s. The material was removed from the batch mixer and compression-molded to a thickness of 1.5 mm at 190 °C for 300 s before being cooled to room temperature. 12 mm disks were then cut from the compression-molded material for further analysis.

**2.2. Thermal–Shear Profile.** A Linkam CSS450 shear cell was used to control the thermal–shear profile. The CSS450 is a parallel plate shearing device in which a small aperture in the base and lid allows

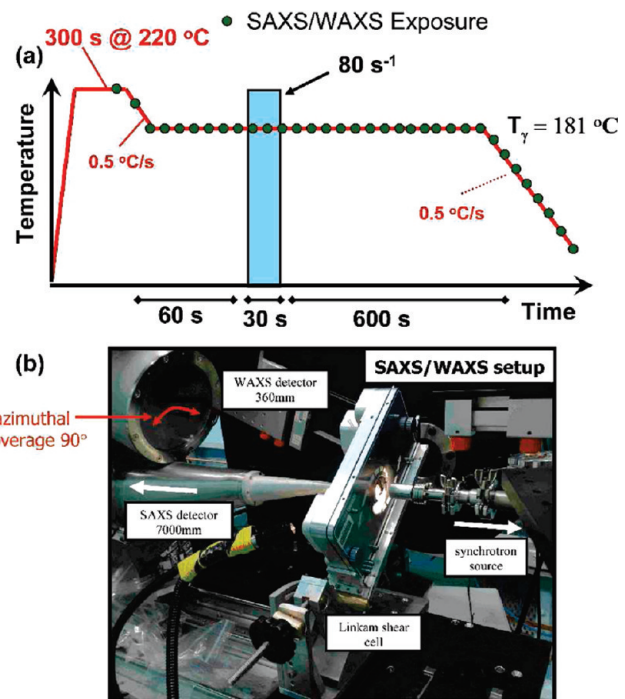


Figure 1. (a) Thermal–shear profile. (b) Experimental setup.

observation of the polymer in situ. The sample temperature was calibrated using external thermocouples inserted into the melt. The influence of wall slip and nonuniform velocity profiles through the thickness of the sample were considered to be comparable for all samples. The thermal–shear profile is shown in Figure 1a. The previously compression-molded disks were heated to 220 °C and compressed slowly to the working distance of 0.25 mm at 0.01 mm/s. The compressed disks were held at the melting temperature for at least 300 s to erase the previous thermal history of the sample. The samples were cooled to the shear temperature ( $T_\gamma = 181^\circ\text{C}$ ) and held for 60 s before a continuous shear pulse was applied to the melt for 30 s at a shear rate of 80 s<sup>-1</sup>. The samples were then held at temperature for a further 600 s before being cooled at 0.5 °C/s to room temperature.

### 2.3. Wide- and Small-Angle X-ray Scattering (SAXS/WAXS).

The shear cell was adapted for use with X-ray radiation. The bottom plate had three slots allowing X-rays to be introduced to the sample. The top plate had a narrow 3 mm diameter aperture allowing scattered X-rays to pass. Thin films of Kapton ~0.05 mm were used to contain the sample between the top and bottom plates. Simultaneous two-dimensional SAXS/WAXS experiments were performed on the SAXS/WAXS beamline at the Australian Synchrotron (Figure 1b). The setup allowed for in situ investigations with a considerable amount of the scattered intensity around the azimuth ( $\varphi \sim 90^\circ$ ) in the WAXS region to be captured, while simultaneously capturing complete 2D SAXS patterns. Details of the SAXS and WAXS detectors used in the experiment are presented in Table 1. Beam dimensions of 0.2 mm × 0.1 mm, a wavelength of  $\lambda = 1.34\text{ \AA}$ , and an exposure time of 1 s were employed throughout the experiment. The time between successive exposures was 5.6 s. Scattering without the specimen was recorded to enable background correction. All images were normalized to the main beam intensity before subtraction. The Nika set of macros for Igor Pro was used to reduce the 2D data. The scattering vector was calculated by the relation  $q = 4\pi \sin \theta / \lambda$ , where  $2\theta$  is the scattering angle.

**2.4. DSC.** Differential scanning calorimetry (DSC) experiments were performed using a Perkin-Elmer DSC-7. Sample size was ~5 mg. Pure indium and zinc references were used for calibration. Samples were run in

**Table 1. Details of the X-ray Detectors Used in This Experiment**

detector	camera length (mm)	count rate (X-ray/s)	azimuthal		
			pixel size (mm)	coverage (deg)	$q$ range ( $\text{\AA}^{-1}$ )
SAXS: Dectris- Pilatus 1M	7300	$>2 \times 10^6$	0.172	$\sim 360$	0.003–0.1
WAXS: MAR- 165	320	$0.4 \times 10^6$	0.080	$\sim 90$	0.5–2.5

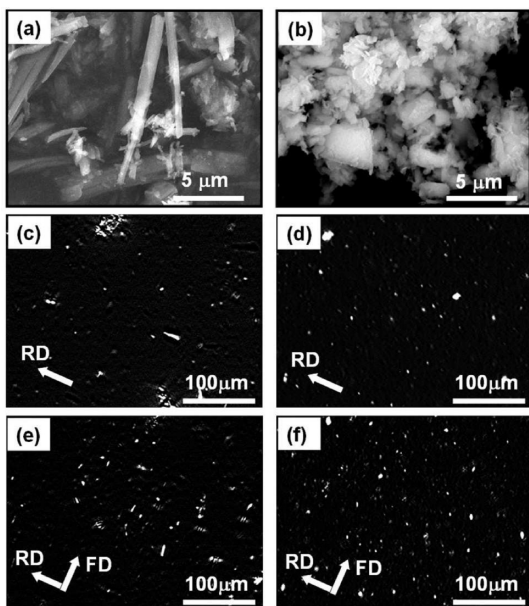


**Figure 2.** Scanning electron micrographs of (a) sodium benzoate (SB) and (b) bicyclo[2.2.1]heptane-2,3-dicarboxylic acid (HPN). Polarized optical micrographs of (c) iPP(1.00SB) and (d) iPP(1.00HPN) in the quiescent condition and (e) iPP(1.00SB) and (f) iPP(1.00HPN) after shear (time = 30 s, shear rate =  $80 \text{ s}^{-1}$ , shear temperature =  $181^\circ\text{C}$ ).

triplicate. Uncertainty in the parameters measured by DSC was assessed by calculating the standard error in the measurement, and the 95.4% confidence interval was reported.

**2.5. Microscopy.** Ex-situ images of the nucleating particles were taken on a JEOL JSM-7001F field emission scanning electron microscope operating in secondary electron mode. Samples were coated to  $10 \text{ \AA}$  thick with gold/platinum and imaged at an acceleration voltage of  $5 \text{ kV}$ . In-situ images of the nucleating particles in the polymer matrix were made under polarized light in the Linkam shear cell using a Nikon 80i microscope and a Nikon DS-Fi1 CCD camera.

### 3. RESULTS

**3.1. Nucleant Particle Characterization.** The morphology of the two nucleant particles before being compounded into the iPP matrix is shown in Figure 2a,b. Standard metallographic techniques were employed to determine the average size and surface area of the two nucleating particles (Table 2). The SB particles were needlelike particles with an aspect ratio  $\sim 10$ . HPN particles were roughly isotropic and had an aspect ratio of  $\sim 1$ . Both SB and HPN particles exhibited flat faceted surfaces. Figure 2c,d shows both SB and HPN particles were well dispersed in the iPP

matrix by the mixing procedures employed. The SB particles showed some preferred orientation of their long axis along the radial direction of the shear cell in the quiescent condition. This alignment is presumably due to the weak flow field applied to the sample when it was compressed in the initial stages of the experiment. After a 30 s shear at a shear rate of  $80 \text{ s}^{-1}$ , both nucleant particles remained well dispersed (Figure 2e,f). After shear the SB particles showed preferred orientation of their long axis along the flow direction.

The nucleation efficiency of the particles was determined according to the method proposed by Fillon et al.<sup>46,47</sup> This method assumes the best nucleators are polymer self-seeds. i.e., small crystal fragments made from the crystals of the polymer. The peak crystallization temperature during continuous cooling of a self-nucleated polymer is considered as the upper bound ( $T_{c2}$ ), while the crystallization temperature of the pure polymer is considered the lower bound ( $T_{c1}$ ). The nucleation efficiency (NE) can then be calculated according to the following equation

$$\text{NE} = \frac{T_{cNA} - T_{c1}}{T_{c2} - T_{c1}} \quad (1)$$

where  $T_{cNA}$  is the crystallization temperature of the polymer samples containing the nucleating particles.

Table 2 shows the influence of loading level of the two nucleating particles on the NE. The NE increased with increasing loading of both nucleating particles. This is simply related to the higher number of heterogeneous sites available for nucleation. HPN was found to be a far superior nucleating particle in terms of raising NE compared to SB, when measured at an equivalent surface area. This result shows that HPN particles have a greater ability to nucleate iPP crystals than SB particles. Indeed, HPN has been shown to have one of the highest NE of all known iPP nucleating agents.<sup>48</sup>

### 3.2. Observation of Shish during and after Shear Flow.

Selected 2D SAXS patterns taken before, during, and after the shear profile are shown in Figure 3. The images shown before shear have had the empty cell data subtracted as the background. Before shear all three samples showed diffuse isotropic scattering profiles consistent with an amorphous iPP melt with no preferred orientation. To enhance scattering contrast for the subsequent 2D SAXS images, both the empty cell and the melt immediately prior to the start of shear were subtracted from all subsequent images. Immediately after the application of shear, a strong increase in equatorial scattering was observed as indicated by the arrows in Figure 3. The increase in equatorial scattering is consistent with the formation of shish aligned along the flow direction. The presence of fibrils in the micrographs of quenched samples verified shish were formed by the imposed thermal–shear profile. After the shear pulse stopped, the equatorial streaks in all samples became weaker and spread around the azimuth. This indicates that the shish are not entirely stable in this temperature regime. Large differences in the scattered intensity were observed between the three samples. The addition of both nucleating particles increased the intensity of the equatorial streak compared to iPP(control). The equatorial streak in iPP(1.00SB) were significantly more intense, extended to higher  $q$  values and where sharper compared to those in iPP(1.00HPN). These differences in scattered intensity will be quantitatively investigated during and after shear in the following section.

In addition to the equatorial scattering, a surprisingly sharp meridional streak was also observed in the SAXS patterns during

**Table 2. Summary of the Morphology of the Sodium Benzoate (SB) and Bicyclo[2.2.1]heptane-2,3-dicarboxylic Acid (HPN) Particles Used in This Investigation and Their Influence on the Quiescent Crystallization of Isotactic Polypropylene (iPP)<sup>a</sup>**

sample	chemical structure	nucleant shape	average dimension ( $\mu\text{m}$ )	loading (wt. %)	particle surface area ( $\text{m}^2/\text{g}$ )	$T_c$ (°C)	NE (%)
iPP(control)	-	-	-	neat	-	111.3(3)	0
iPP(self seed)	-	-	-	self seed	-	142.7(3)	100
iPP(0.05SB)		needle	0.43(4) x 4.70(17)	0.05	0.005	113.3(3)	6(1)
iPP(0.10SB)				0.10	0.010	114.5(3)	11(1)
iPP(0.50SB)				0.50	0.052	119.4(3)	26(1)
iPP(1.00SB)				1.00	0.103	120.6(3)	30(1)
iPP(0.05HPN)		isotropic	0.41(4)	0.05	0.007	124.8(3)	43(1)
iPP(0.10HPN)				0.10	0.014	127.2(3)	49(1)
iPP(0.50HPN)				0.50	0.071	129.7(3)	54(1)
iPP(1.00HPN)				1.00	0.141	132.8(3)	59(1)

<sup>a</sup>  $T_c$  = peak crystallization temperature, NE = nucleation efficiency.

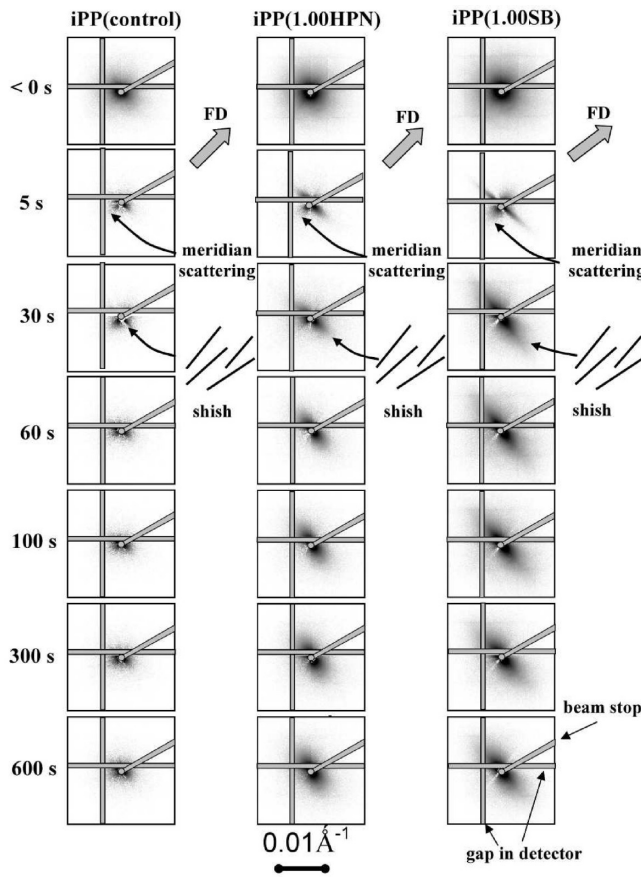


**Figure 3.** Selected small-angle X-ray scattering patterns taken at various stages before, during, and after continuous shear (shear time = 30 s, shear rate = 80  $\text{s}^{-1}$ , shear temperature = 181 °C).

shear for all samples. Furthermore, the meridional streak disappeared soon after the shear stopped. To further investigate this anomalous feature, the intensity profile around the azimuth was determined between scattering vectors  $0.003 \leq q \leq 0.01 \text{ \AA}^{-1}$ . Distinct equatorial

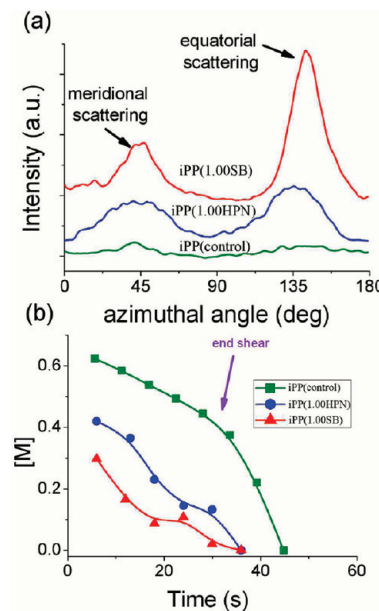


**Figure 4.** (a) Plot of background subtracted intensity versus azimuthal angle during the first 5 s of shear. (b) Relative proportion of meridional scattering ( $[M]$ ) during and immediately after shear (shear time = 30 s, shear rate =  $80 \text{ s}^{-1}$ , shear temperature = 181 °C).

and meridional peaks were clearly evident in all profiles during shear (Figure 4a). The relative amount of meridional scattering ( $[M]$ ) was estimated during shear flow using the following equation

$$[M] = \frac{A_m}{A_m + A_e} \quad (2)$$

where  $A_m$  and  $A_e$  are the areas of the azimuthally integrated meridional and equatorial peaks. The results are plotted in Figure 4b. For all samples the amount of meridional scattering decreased steadily during shear and disappeared altogether soon after the shear ended.

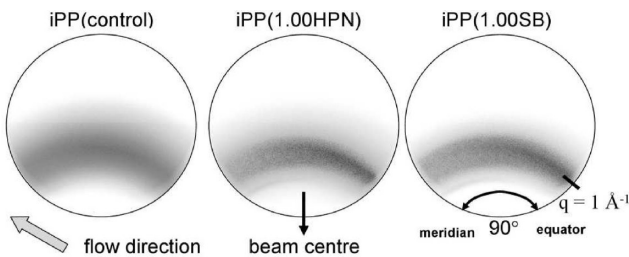


**Figure 5.** Raw wide-angle X-ray scattering patterns taken just prior to the end of continuous shear (shear time = 30 s, shear rate = 80 s<sup>-1</sup>, shear temperature = 181 °C).

The WAXS patterns before shear showed an unoriented diffuse amorphous halo with peak intensity near  $q = 1 \text{ \AA}^{-1}$ , further confirming that the melt was unoriented prior to shear. The application of shear did not induce any crystalline scattering during or for at least 600 s after the shear had stopped. This shows that the scattering observed in the SAXS images is due to noncrystalline entities. However, during shear flow some preferred orientation of the amorphous halo became evident with an increase in intensity occurring toward the equator at  $q \sim 1 \text{ \AA}^{-1}$  (Figure 5). The interpretation of amorphous orientation from WAXS is uncertain in this case due to the complex combination of inter- and intrachain interactions. Nevertheless, the observed increase in preferred orientation with the addition of both nucleating particle is consistent with the results presented in Figure 3.

**3.3. Quantitative Investigation of Shish during and after Shear Flow.** The behavior of the shish during and after shear was further probed by determining the integrated scattered intensity from the equatorial scattering streak in the SAXS images ( $I_{\text{shish}}$ ) according to the following equation:

$$I_{\text{shish}} = \int_{0.003}^{0.3} \int_{0^\circ}^{20^\circ} I(q, \varphi) dq d\varphi \quad (3)$$

$I_{\text{shish}}$  determined in this way is proportional to the total volume of shish ( $v_{\text{shish}}$ ) and the magnitude of their density contrast to the surrounding melt ( $\Delta\rho_{\text{shish-melt}}$ ). The results of this analysis are plotted in Figure 6. All samples showed the same general behavior. During shear,  $I_{\text{shish}}$  initially increased rapidly, reaching a peak value just prior to the shear pulse ending. This indicates that steady-state conditions were only achieved toward the end of the shear profile. The magnitude of  $I_{\text{shish}}$  was substantially larger in iPP(1.00HPN) and iPP(1.00SB) compared to iPP(control), raising the magnitude of  $I_{\text{shish}}$  by a factor of 5 and 7, respectively. The higher value of  $I_{\text{shish}}$  indicates that the addition of nucleating particles increased the volume fraction of shish or their density contrast. However, large changes in the density contrast of the shish is considered less likely when taken in conjunction with measurements of the shish dimensions which are discussed subsequently.

Immediately after the shear pulse stopped,  $I_{\text{shish}}$  began to exponentially decay to an interim lower plateau level. This indicates that some shish are unstable and relax back into the melt, while other shish have some stability at the experimental temperature. The decay constant ( $\tau_{\text{shish}}$ ) between peak  $I_{\text{shish}}$  and the lower plateau was approximated by a simple exponential decay model:

$$I_{\text{shish}}(t) = I_{\text{shish}(0)} + \Delta I_{\text{shish}} e^{-t/\tau_{\text{shish}}} \quad (4)$$

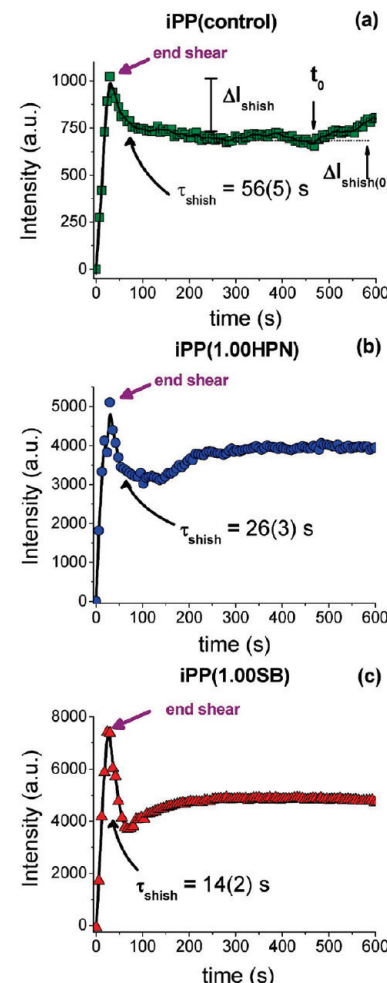


**Figure 6.** Scattered intensity from shish ( $I_{\text{shish}}$ ) during and after shear for (a) iPP(control), (b) iPP(1.00HPN), and (c) iPP(1.00SB) (shear time = 30 s, shear rate = 80 s<sup>-1</sup>, shear temperature = 181 °C).

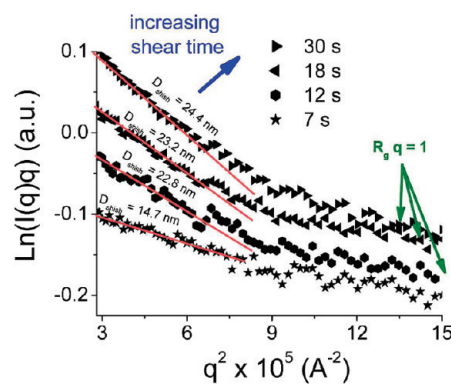


**Figure 7.** Guinier plot of  $\ln(I(q)/q)$  versus  $q^2$  showing selected lines during shear flow for iPP(control) (shear rate = 80 s<sup>-1</sup>, shear temperature = 181 °C).

where  $I_{\text{shish}(0)}$  and  $\Delta I_{\text{shish}}$  are illustrated in Figure 6. Compared to iPP(control), the addition of both nucleating particles was found to decrease  $\tau_{\text{shish}}$ .

After an induction time ( $t_0$ ) at the lower plateau level, the value of  $I_{\text{shish}}$  began to increase again before reaching an upper plateau level.

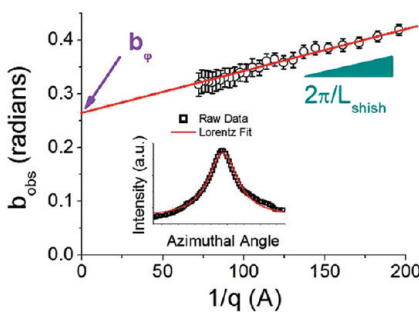


**Figure 8.** Plot of azimuthal integral breadth ( $b_{\text{obs}}$ ) as a function of  $1/q$  showing the method used to separate out the contributions of the misorientation of shish ( $b_{\phi}$ ) and the shish length  $L_{\text{shish}}$  at low scattering vectors ( $q$ ). Inset shows a typical background corrected azimuthal intensity profile fitted with a Lorentz function.

The value of  $I_{\text{shish}}$  was then stable until the end of the isothermal hold. The addition of both nucleating particles decreased this induction time compared to iPP(control) ( $t_0 = 476(3)$  s), with iPP(1.00SB) ( $t_0 = 68(3)$  s) having a shorter  $t_0$  than iPP(1.00HPN) ( $t_0 = 138(3)$  s). This increase in  $I_{\text{shish}}$  could be due to an increase in the volume fraction of shish or changes in their density contrast. To further understand this interesting phenomenon, the dimensions of the shish during and after shear flow are determined.

The diameter of the shish was estimated by applying the Guinier approximation<sup>49</sup> to a 20° arc in the azimuthal direction and centered on the maximum intensity of the equatorial scattering streak. The radius of gyration ( $R_g$ ) of rodlike scatterers can be approximated from the gradient of the linear region at low  $q$  of a plot of  $\ln(I(q)q)$  versus  $q^2$  according to the equation

$$I \propto \frac{1}{q} e^{-R_g^2 q^2/2} \quad (5)$$

Assuming the shish show cylindrical symmetry, the diameter of the shish is

$$D_{\text{shish}} = 8^{1/2} R_g \quad (6)$$

Strictly speaking, the Guinier approximation used in this way is only true for the central part of the scattering from a dilute (and therefore uncorrelated) solution of rods. However, it has been applied successfully to estimate the diameter of shish in previous studies.<sup>24,40</sup> Selected Guinier plots for iPP(control) during shear are shown in Figure 7. For all scattering patterns the plot consisted of two linear regions with the transition occurring at  $q = 0.094$  Å<sup>-1</sup>. The first region (i.e.,  $q < 0.094$  Å<sup>-1</sup>) was used to determine  $D_{\text{shish}}$  since the second region should be discarded as the Guinier approximation is only valid in the small angle limit where the criteria  $R_g q < 1$  is maintained.

The average length of the structural units along the long axis of the shish ( $L_{\text{shish}}$ ) and their alignment along the flow direction ( $b_{\phi}$ ) can be determined using the method proposed by Perret and Ruland.<sup>50</sup> The underlying basis for the method is that at low  $q$  the contribution from the misorientation of the scatterers should be constant, while the contribution from the length of the scatterers should depend on  $q$ . The proposed method consists of determining the integral breadth of a series of azimuthal profiles taken at different values of  $q$  along the equator. The integral breadth ( $b_{\text{obs}}$ ) is defined according to the equation

$$b_{\text{obs}}(q) = \frac{1}{I(q, \pi/2)} \int_{-\pi/2}^{\pi/2} I(q, \varphi) d\varphi \quad (7)$$

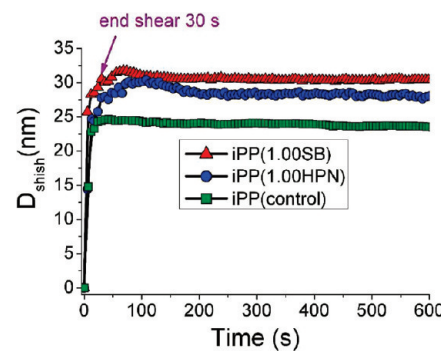


**Figure 9.** Calculated diameter of shish ( $D_{\text{shish}}$ ) during and after shear (shear time = 30 s, shear rate = 80 s<sup>-1</sup>, shear temperature = 181 °C).

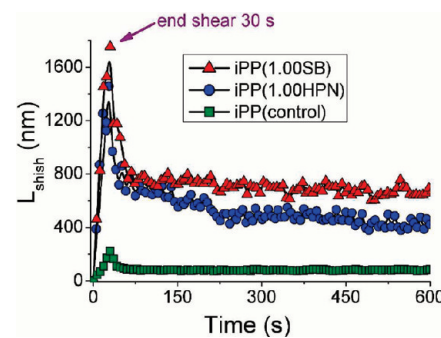


**Figure 10.** Calculated length of shish ( $L_{\text{shish}}$ ) during and after (shear time = 30 s, shear rate = 80 s<sup>-1</sup>, shear temperature = 181 °C).

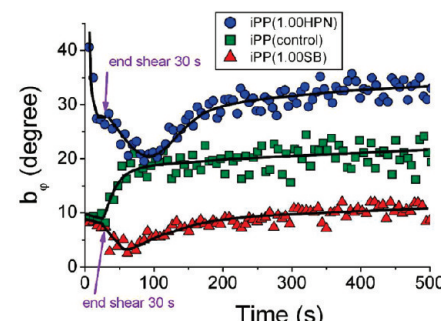


**Figure 11.** Calculated shish misorientation ( $b_{\phi}$ ) during and after shear (shear time = 30 s, shear rate = 80 s<sup>-1</sup>, shear temperature = 181 °C).

where  $\varphi$  is the azimuthal angle and  $I(q, \varphi)$  is the background-corrected intensity. For a Cauchy-like (Lorentz) orientation distribution of scatterers,  $b_{\text{obs}}$  is then related to  $b_{\phi}$  and  $L_{\text{shish}}$  by

$$b_{\text{obs}} = b_{\phi} + \frac{2\pi}{L_{\text{shish}} q} \quad (\text{Lorentz}) \quad (8)$$

For a Gaussian orientation distribution of scatters the equation becomes

$$b_{\text{obs}}^2 = b_{\phi}^2 + \frac{4\pi^2}{L_{\text{shish}}^2 q^2} \quad (\text{Gaussian}) \quad (9)$$

In the present work it was found that the Lorentz function best fit the observed azimuthal intensity profile, and  $b_{\phi}$  and  $L_{\text{shish}}$  were determined from a plot of  $b_{\text{obs}}$  versus  $1/q$  (Figure 8). The

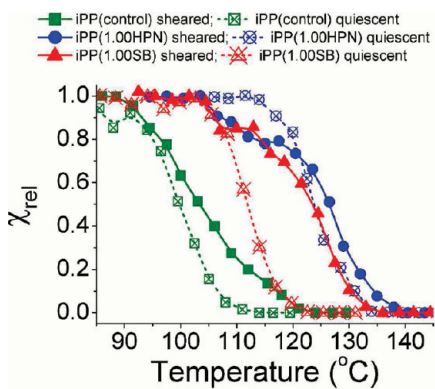


**Figure 12.** Influence of nucleating particle and shear condition on the crystallization during continuous cooling (shear time = 30 s, shear rate =  $80 \text{ s}^{-1}$ , shear temperature =  $181^\circ\text{C}$ , hold time = 600 s, cooling rate =  $0.5^\circ\text{C}/\text{s}$ ).

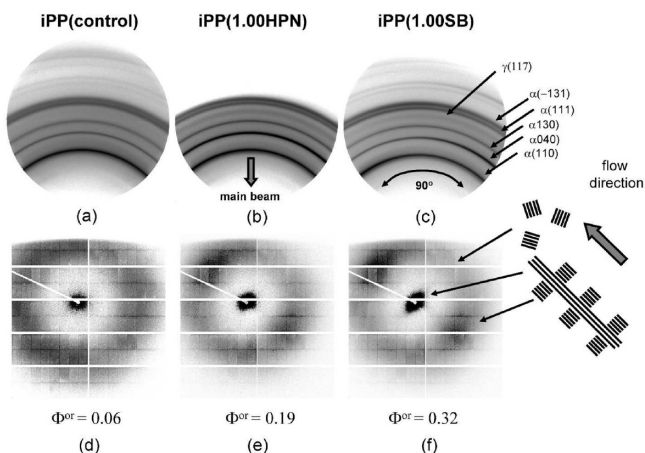


**Figure 13.** Small- and wide-angle X-ray scattering patterns in the fully crystallized condition taken at room temperature. (a, d) iPP(control), (b, e) iPP(1.00HPN), (c, f) iPP(1.00SB). Oriented fraction of lamellae ( $\Phi^{\text{or}}$ ) (shear time = 30 s, shear rate =  $80 \text{ s}^{-1}$ , shear temperature =  $181^\circ\text{C}$ , hold time = 600 s, cooling rate =  $0.5^\circ\text{C}/\text{s}$ ).

magnitude of  $L_{\text{shish}}$  for all samples was below 2000 nm, which is smaller than the typical shish length observed using microscopy methods. However, it should be noted that the quantity  $L_{\text{shish}}$  represents the average coherence length of the structural units along the long axis of the shish, which will be different from that measured by microscopic methods.

The time evolution of the shish dimensions  $D_{\text{shish}}$  and  $L_{\text{shish}}$  are presented in Figures 9 and Figure 10, respectively. In all three samples both  $D_{\text{shish}}$  and  $L_{\text{shish}}$  were found to increase rapidly with increasing shear time. After shear,  $L_{\text{shish}}$  decreased quickly to an interim value and then decreased more slowly until the end of the isothermal hold.  $D_{\text{shish}}$ , on the other hand, at first kept increasing after the shear had stopped, reaching an upper plateau level.  $D_{\text{shish}}$  then began to decline from the upper plateau with increasing time until the end of the isothermal hold. The addition of both nucleating particles led to a large increase in the value of  $L_{\text{shish}}$  and a small increase in the value of  $D_{\text{shish}}$ . The magnitudes of  $D_{\text{shish}}$  and  $L_{\text{shish}}$  were larger in iPP(1.00SB) compared to iPP(1.00HPN).

The alignment of shish during and after shear is shown in Figure 11. A line through the middle of the data is included to aid interpretation. A lower value of  $b_\phi$  indicates a higher shish alignment along the flow direction. During shear, iPP(control) started with high alignment along the flow direction which then increased slightly as shear progressed. At the beginning of shear the shish in iPP(1.00HPN) had low alignment along the flow direction. However, as shear progressed, their alignment increased substantially. At the beginning of shear the shish in iPP(1.00SB) were highly aligned along the flow direction. Further shear increased their alignment further. After shear stopped, the shish alignment in iPP(control) immediately decreased. Conversely, the alignment of shish in the iPP containing both nucleating particles increased after shear stopped, reaching a lower plateau before rising again with increasing time. In general, the relative alignment of shish for the three samples went iPP(1.00SB) > iPP(control) > iPP(1.00HPN).

**3.4. Crystallization of Sheared and Relaxed iPP Containing Nucleating Particles.** At the end of the 600 s hold, the samples were cooled to room temperature at  $0.5^\circ\text{C}/\text{s}$ . The volume crystallinity index ( $\chi_v$ ) was measured from the circular integration of WAXS patterns during cooling according to the method described in a previous paper.<sup>42</sup> The relative crystallinity ( $\chi_{\text{rel}}$ ), defined as the instantaneous crystallinity divided by the room temperature crystallinity, was then plotted as a function of temperature (Figure 12). The results were compared to samples that had undergone the same thermal profile but were not sheared. Without shear, the crystallization progressed according to the relative nucleation efficiencies of the added particles. With shear, all samples showed an increase crystallization temperature compared to the samples which had not been sheared. This is consistent with the formation of shear-induced nuclei which provide extra nucleation sites for crystal nucleation. iPP(1.00SB) showed the largest change in the crystallization kinetics after shear, consistent with the higher numbers of shish observed before the onset of crystallization. iPP(1.00HPN) exhibited the smallest change in crystallization kinetics, which is presumably due to the high nucleation efficiency of the HPN particles swamping crystallization under quiescent conditions.

Simultaneous SAXS/WAXS patterns of the sheared samples obtained in the fully crystallized state are shown in Figure 13. The WAXS patterns of all samples showed crystalline reflections consistent with the formation of only  $\alpha$ -iPP and  $\gamma$ -iPP crystals. In pure iPP it is known that shear flow can induce  $\beta$ -iPP as long as the kinetic requirement for a higher  $\beta$ -iPP growth rate than  $\alpha$ -iPP is achieved (i.e., between  $105$  and  $141^\circ\text{C}$ <sup>51</sup>). Therefore, the absence of  $\beta$ -iPP reflections for iPP(control) in this experiment was surprising, given that crystal nucleation occurred within this temperature range. The absence of  $\beta$ -iPP is even more intriguing, given that in a previous study shear-induced formation of  $\beta$ -iPP was observed in the same polymer.<sup>42</sup> In that study isothermal crystallization (crystallization temperature =  $135^\circ\text{C}$ ) was carried out after a moderate step shear (shear rate =  $80 \text{ s}^{-1}$ , shear time = 1 s). These conditions are substantially different from those used in this study. Indeed, it is worthwhile to note that in many of the studies presented in the literature shear-induced formation of  $\beta$ -iPP has been investigated after the application of a brief shear pulse and where crystallization occurred under isothermal conditions. Although not in the scope of the present study, further work is planned to clarify the reason for the absence of  $\beta$ -iPP in iPP(control).

The  $\gamma$ -iPP crystallinity ( $\chi_\gamma$ ) of the fully crystallized material was determined using the Turner-Jones method:<sup>52</sup>

$$K_\gamma = \frac{A_\gamma(117)}{A_\gamma(117) + A_\alpha(130)} \quad (10)$$

$$\chi_\gamma = K_\gamma \chi_v \quad (11)$$

where  $A_\alpha(130)$  and  $A_\gamma(117)$  are the integrated areas of the crystalline reflections indicated in Figure 13. The addition of both nucleating particle significantly increased  $\chi_\gamma$  from 0.02 in iPP(control) to 0.11 in iPP(1.00SB) and 0.17 in iPP(1.00HPN). The promotion of  $\gamma$ -iPP in the samples containing the nucleants is thought to be related to the substantially higher density of nuclei in these samples (both shear-induced and heterogeneous sites on the surface of the particles), combined with the relatively fast cooling rate which would further increase the number of active nuclei. The high density of nuclei would lead to multiple nucleation events occurring simultaneously along a chain, thereby reducing the time available for the chain to properly organize during the initial crystallization. Combined with the stereo- and regio-defects already present along the polymer backbone, this would promote shorter isotactic sequences during crystallization. It has been reported that  $\gamma$ -iPP is favored when the isotactic sequence length is interrupted.<sup>53</sup>

The SAXS/WAXS patterns in Figure 13 show preferred orientation consistent with the shish inducing the formation of kebab structures. In the SAXS region broad lobes were observed along the meridian (kebabs) while equatorial scattering was observed at low  $q$  (shish). Increases in scattered intensity along the equator for the  $\alpha(110)$ ,  $\alpha(040)$ , and  $\alpha(130)$  reflections in the WAXS region indicated significant crystalline  $c$ -axis orientation along the flow direction. The oriented fraction of lamellae ( $\Phi^{\text{or}}$ ) was determined from the SAXS pattern according to the method presented in a previous paper.<sup>42</sup> The addition of both nucleating particles increased  $\Phi^{\text{or}}$ , with SB having almost twice the number of oriented lamellae compared to HPN. The samples were reheated to 220 °C and was held there for a further 300 s. Upon cooling, no preferred orientation was observed in any sample. This shows that the particles themselves did not template oriented crystal growth.

## 4. DISCUSSION

**4.1. Formation of Shish during Shear.** Shish formation during shear flow is of considerable practical importance as shish promote oriented hierarchical structures, which significantly alter the physical, optical, and mechanical properties of the solid polymer. However, the shish formation mechanism is still under intense debate. The proposed mechanisms broadly fall into three groups: shish form directly from extended chains (or chain segments) produced via an abrupt coil-to-stretch transition;<sup>1,5,6,11</sup> shish nucleate from pre-existing nuclei and then grow by the addition of new chain segments;<sup>12–17</sup> and shish form in discrete steps, by the aggregation of discrete nuclei into oriented threads.<sup>18–22</sup> These three mechanisms are not necessarily mutually exclusive, and more than one mechanism could lead to shish formation under a given set of processing conditions.

Keller et al.<sup>1,50,54</sup> explained shish formation around the coil-to-stretch transition originally proposed by de Gennes<sup>55</sup> for dilute polymer solutions. In the model, shear flow results in the abrupt unravelling of the longest chains in the system. These extended

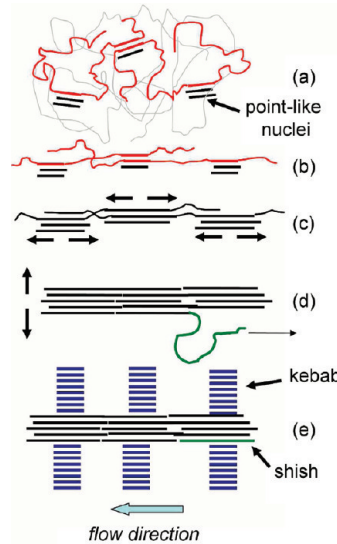


**Figure 14.** Mechanism of shish formation. (a) Formation of shear-induced pointlike nuclei. (b) Aggregation of pointlike nuclei into oriented thread when the tie molecules are pulled taut by shear flow. (c) Infill growth of aligned pointlike nuclei to form shish. (d) Growth of shish in the lateral direction by the unravelling of adsorbed chains along the length of the shish. (e) Nucleation of chain folded kebabs on lateral surface of shish.

chains then migrate together and undergo densification into the final shish structure. Chains that were not elongated by the flow field form the kebabs during subsequent crystallization. Hsiao et al.<sup>5</sup> extended this model by noting that in an entangled melt it may not be the whole chain which would become extended but rather the sections of chain between entanglement points.

Pennings et al.<sup>12,56</sup> suggested that chains adsorb onto the surface of pre-existing nuclei which then allows the free end to be extended by the flow field. This leads to longitudinal growth of the nuclei. Therefore, in the scenario an external flow field was thought to be required for shish growth. Studying deformed films of isotactic polystyrene, Petermann et al.<sup>17</sup> observed the presence of obstacles altered the shish growth direction. This observation implies that shish may also grow without a shear field by an autocatalytic process at the ends of the shish. Nevertheless, the presence of an external flow field would further enhance alignment of chain sections, increasing growth rates.

An aggregation-type mechanism for shish formation was first proposed by Hoffman,<sup>21,22</sup> who argued that kebabs are nucleated at specific sites along the core of the shish and that these provide information about structural singularities in the backbone of the shish. In this work, the shish were thought to originate with the aggregation of multiple pointlike nuclei along the length of a flow elongated molecule. In the case of iPP these pointlike nuclei can be thought of as small bundles of roughly parallel chains in helical conformations which show intermediate order between amorphous and crystalline states.<sup>57</sup> Janeschitz-Kriegl et al.<sup>2,18</sup> provided further evidence for an aggregation type mechanism by noting that the number of pointlike nuclei varied nonlinearly with the mechanical work during shear flow. This observation implies the existence of long-range interactions between pointlike nuclei. Heeley et al.<sup>20</sup> suggested this interaction could occur if the pointlike nuclei act as anchor points along the length of a molecule, allowing flow to more effectively orient the molecule, and thus the attached pointlike nuclei. An alternative mechanism

**Table 3. Empirical Disengagement ( $\tau_d$ ) and Chain Rouse ( $\tau_R$ ) Times for Stretched iPP Molecules in a Monodisperse Entangled Melt Held at 181 °C**

relaxation times (s)	$M_w$ (367 000 g mol <sup>-1</sup> )	$M_{(>99\%)}^{(3673 000 g mol^{-1})^a}$
$\tau_d$	0.0443	63.64
$\tau_R$	0.0003	0.0270

<sup>a</sup> Molecular weight calculated from a log-normal fit of the molecular distribution.

was proposed by Seki et al.,<sup>19</sup> who suggested that molecules which adsorb onto the surface of pointlike nuclei would get rapidly extended along the flow direction. New pointlike nuclei would then form from these extended chain segments. Nevertheless, the aggregation of pointlike nuclei into oriented threads has until now not been observed.

During shear flow, meridional scattering streaks were observed in the SAXS patterns of all samples investigated, in conjunction with equatorial streaks. A review of the available literature indicates that such meridional scattering has not been previously observed during shear flow. Similar SAXS/WAXS investigations by Soman et al.<sup>58</sup> on sheared iPP have shown the formation of meridional scattering after an appreciable induction time and following the cessation of shear. In that work the meridional scattering was explained by the formation of noncrystalline kebabs. However, the lack of any appreciable induction time for the formation of the meridional peaks as well as the high temperature used in this experiment, which was ~15 °C higher than the lamellae melting temperature, would make this scenario unlikely. Consequently, the most likely structures that fit the observed scattering are highly aligned discrete nuclei. Such a structure would be consistent with shish forming, in discrete steps by the aggregation of pointlike nuclei into oriented threads. The suggested sequence of events is schematically illustrated in Figure 14.

Meridional scattering is not commonly observed in the SAXS patterns of sheared semicrystalline polymers, and therefore its presence in this experiment needs further explanation. The relative proportion of meridional scattering was observed to decrease during shear flow (Figure 4). Furthermore, the meridional scattering disappeared soon after the shear was stopped. This can be explained by the infill of regions between neighboring aligned pointlike nuclei which would be promoted by the highly extended chains between the nuclei. Such infill growth could be aided by the autocatalytic mechanism proposed by Peterman et al.<sup>17</sup> This highlights that the meridional scattering may only be apparent during shear flow, while the shish are forming. However, because of the fast kinetics, many experiments previously presented in the literature investigated shish formation after shear flow stopped. Accordingly, it is the high shear temperature used in this experiment which slows down the formation of shish, in combination with the relatively long shear times, which allows shish formation to be investigated.

The increase in  $D_{shish}$  during shear shows that the shish can also grow in the lateral direction during shear flow. Yamazaki et al.<sup>15</sup> suggested that this could occur by the repeated adsorption of chain ends to the shish surface. Once pinned on the surface, the free ends of the chain would then be rapidly elongated along the surface of the shish by the shear field. This result highlights

that more than one mechanism is responsible for shish growth during shear.

**4.2. Stability of Shish after Shear.** Immediately after the shear pulse ended the shish began to dissolve back into the melt. At least two separate steps are thought to be necessary for this to occur. The first step is the detachment of a stem from the surface of the shish (melting). Once detached, the extended stem can then relax in a snakelike motion along an imaginary tube formed by the constraints imposed by neighboring molecules to restore its equilibrium conformation (reptation). The disengagement ( $\tau_d$ ) and the chain Rouse times ( $\tau_R$ ) of a stretched molecule were empirically determined using the Doi–Edwards model:<sup>59</sup>

$$\tau_d = 3\tau_e Z^3 [1 - \kappa Z^{-0.5}]^2 \quad (12)$$

$$\tau_R = \tau_e Z^2 \quad (13)$$

where  $\tau_e$  is the Rouse time of a single entanglement strand ( $\tau_e = 5.42 \times 10^{-8}$  s at 181 °C),  $Z$  is the number of entanglements per chain, and  $k$  is a constant found to be close to unity.<sup>60</sup> Table 3 shows the empirical disengagement and Rouse times for chains with the weight-average molecular weight and the molecular weight above which 1% of the chain population by weight resides. These empirical relaxation times are expected to be an upper bound. This is due to the likely influence of constraint release from the faster relaxation of the shorter chains in the polydisperse melt, which would increase the relaxation rates. For stretched chains which are of the weight-average molecular weight, relaxation occurs rapidly and within a fraction of a second. However, for the longest 1% of chains the relaxation rates are much slower and are comparable to the relaxation rate of  $I_{shish}$  observed for iPP(control) shown in Figure 6. This result is therefore consistent with the view that the dissolution of shish is controlled by the reptation of the high molecular weight component.<sup>23</sup>

Although relaxation processes have been extensively studied in a wide range of polymers, the influence of foreign particles has received comparatively little attention. Previous studies have suggested that the surface of large particles could stabilize extended chain conformations due to the surface contact points acting as physical cross-links.<sup>40,41,61</sup> Similarly, molecularly dispersed nanoparticles, which have a strong affinity for the polymer molecule, could increase the number of physical cross-links in an analogous way.<sup>25,43,62</sup> However, in the present experiment the addition of both nucleating particles was surprisingly found to increase the initial rate of relaxation of shish after shear ended, contrary to these expectations.

It is proposed that this surprising increase in shish relaxation in the presence of particles can be explained by the polydisperse nature of the iPP matrix. It is widely considered that when a polydisperse polymer is sheared, it is the longest chains which are the first to be involved in the formation of shish.<sup>5,11,19,63</sup> Recent small-angle neutron scattering studies (SANS) have indicated that the longer chains are not necessarily over represented in the shish.<sup>14</sup> Rather, the longer chains only act to accelerate shish formation, recruiting out chains smaller chains to the forming shish. The presence of longer molecular weight chains in the shish structure may also act to stabilize the shish structure once formed by decreasing both the rate of chain detachment from the lateral surface of the shish and subsequent chain relaxation. The molecular weight effect can be explained by the increase in the number of intrachain contact points with increasing chain length. Higher numbers of intrachain contact points then

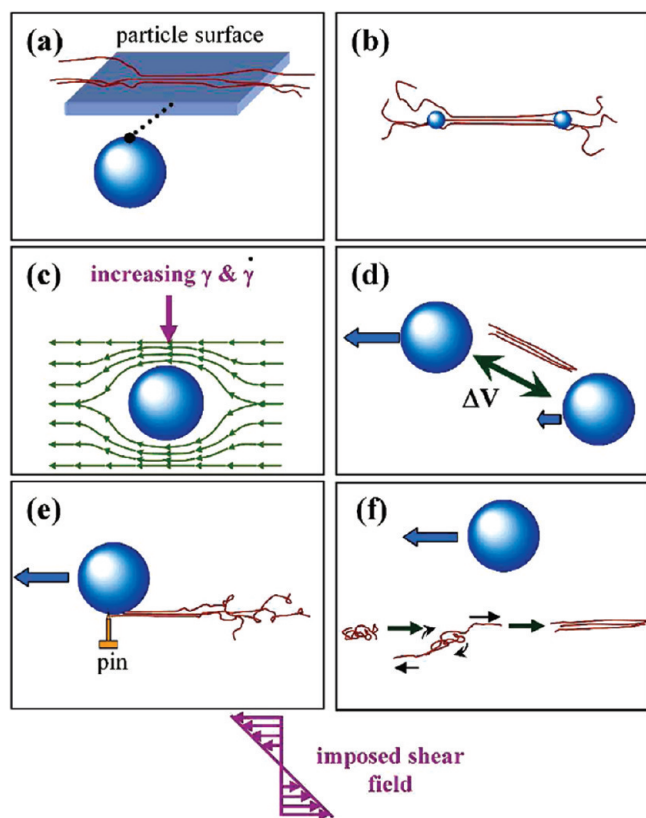


**Figure 15.** Schematic representation of six possible mechanisms for particle-assisted shish formation. (a) Stabilization of extended conformations on the surface of particles. (b) Retard relaxation of extended conformations by increasing the number of physical cross-links. (c) Increased strain and strain rate near the particle caused by flow of matrix around the particle. (d) Separation of nearby particles leading to increased elongation flow between the two particles. (e) One end of a molecule is adsorbed and pinned on the surface of particle, while the other end is extended by shear flow. (f) Long-range perturbation of a molecule's streamline by the motion of a passing particle. Refer to text for more details.

stabilize the extended chain conformations, retarding relaxation. Therefore, the faster relaxation of shish strongly suggests that the presence of the particles decreased the size of chains which could template shish formation. Shish formed around these lower average molecular weight chains would then have a greater propensity to relax than shish that are formed around the higher molecular weight chains.

$I_{\text{shish}}$  was found to increase again after an appreciable induction time. Keum et al.<sup>24</sup> recently observed a similar phenomenon in sheared UHMWPE/HDPE, noting the shish length increased around the same time. Keum then explained the increase in  $I_{\text{shish}}$  by the longitudinal growth of shish using the autocatalytic growth mechanism proposed by Peterman et al.<sup>17</sup> However, in this experiment both  $D_{\text{shish}}$  and  $L_{\text{shish}}$  were observed to decrease over this time period, and therefore autocatalytic growth of shish after shear cannot explain the observed increase in  $I_{\text{shish}}$ . Another possible explanation for the observed increase in  $I_{\text{shish}}$  could be the decomposition of the melt by a spinodal liquid–liquid phase separation, such as proposed by Olmsted et al.<sup>64</sup> Shear is considered to increase the kinetics of the spinodal transformation. Therefore, the observed decrease in the induction time with the addition of nucleating particles would support such a

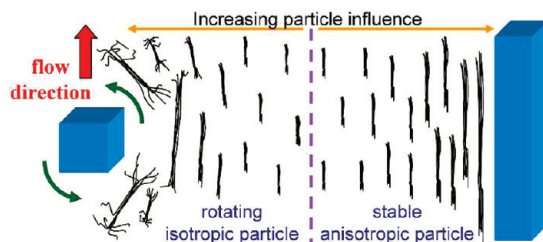


**Figure 16.** Influence of rotating isotropic and stable anisotropic particles on formation of shish.

hypothesis, as the particle's presence appears to increase the intensity of the shear field.

**4.3. Particle-Assisted Shish Formation.** In the present work, both particles were found to increase the amount of shish and their dimension compared to iPP(control). This resulted in a substantially greater crystalline and lamellar orientation during subsequent crystallization. The addition of foreign particles in a wide range of polymer/particle systems has been shown to increase the molecular orientation under shear-induced crystallization conditions.<sup>15,16,25,28,35,38–43</sup> Figure 15 summarizes six possible mechanisms for particle-assisted shish formation. The SAXS results presented in the previous section indicate that the addition of both particles increased the relaxation rate of shish. Therefore, mechanisms where the particles stabilize extended chain conformations would appear to be unlikely to account for the observed increase in shish. Rather, the increased relaxation rate shows that the addition of particles allowed shorter chains to template shish formation. This implies that it is the modification of the strain environment at or near the particle surface which aids shish formation in these materials.

The modification of the local strain environment could occur in at least four ways. Hwang et al.<sup>65</sup> advocated that polymer molecules flow around the particles, and this leads to an increase in both the strain and strain rate near the exposed sides of the particle. Furthermore, Hwang suggested the elongational component of the shear flow would be increased in the region between two separating particles. Jerschow and Janeschitz-Kriegl<sup>35</sup> proposed that polymer molecules may adsorb onto the surface of foreign particles, pinning one end of the molecule. During subsequent shear flow, the free end of the molecule becomes stretched, accelerating the formation of shish. Yamazaki et al.<sup>15,16</sup> investigated the influence of dust on shish formation and drew a similar conclusion. Under simple shear flow, the rotational component of the flow is just sufficient to counteract the elongation component from stretching out the polymer chains. Harlen and Koch<sup>66</sup> showed that polymer molecules moving past particles can tip this balance in the favor of the extensional component. As a molecule moves past a particle, the molecule gets disturbed from its initial streamline due to the slightly different flow histories along the length of the molecule. The molecule now lies over a broader range of streamlines and is able to interact more strongly with the flow and stretch along the flow direction.

The two nucleating particles in this experiment had similar chemical compositions and size. However, both particles had significantly different nucleation efficiencies and aspect ratios. Particles with high affinity for the polymer molecules<sup>25</sup> and high aspect ratios<sup>36</sup> have been suggested to aid the formation of shear-induced nuclei. In this experiment the HPN particles were

relatively isotropic but had a much higher nucleation efficiency than the high aspect ratio SB particles. Compared to the addition of HPN particles, the addition of SB particles resulted in more shish which also had larger dimensions. Therefore, the aspect ratio appears to be the more dominant factor in aiding shish formation rather than nucleation efficiency. An appreciable influence of nucleation efficiency would have suggested a surface mechanism may be important. Hence, the results presented here suggest that the addition of foreign particles assist shish formation by modifying the local strain environment near but not necessarily on the particle surface.

Further information regarding how particle aspect ratio influences shish formation can be gleaned from the development of shish alignment during shear flow. At the start of shear, the shish in iPP(control) and in iPP(1.00SB) were highly aligned along the flow direction, while the shish in iPP(1.00HPN) were not. This result can be explained by how the different particles interact with and particularly how they rotate in the shear field. The orientation of the particle can be described by a family of closed curves known as Jeffery orbital's which depend on the initial orientation of the particles to the flow direction.<sup>67</sup> Furthermore, the rate of rotation is known to depend on the aspect ratio of the particle, with higher aspect ratio particles rotating less than low aspect ratio particles.<sup>68–70</sup> This low rotation rate is consistent with the SB particles being oriented with their long axis along the flow direction (Figure 2e). The higher rotation of the HPN particles could cause shish which are forming nearby to tumble, destabilizing their formation and leading to fewer and smaller shish being formed (Figure 16). Conversely, the SB particles, which adopt a more stable orientation along the flow direction, help guide shish growth. It is interesting to note that the shish alignment in iPP(1.00HPN) dramatically increased during shear. This could indicate that as the shish form, the growing shish stabilize the rotation of the HPN particles, further enhancing their alignment along the flow direction. However, the details of this interesting occurrence remain open for debate.

## 5. CONCLUSIONS

The formation and relaxation of shish was investigated in pure isotactic polypropylene (iPP(control)) and iPP containing two commercial nucleating particles during and after moderate shear flow. The findings from this study are briefly summarized as follows.

Surprising sharp meridional streaks were observed in conjunction with equatorial streaks in the small-angle X-ray scattering patterns during shear flow. As shear progressed, the meridional streak decreased and disappeared soon after the shear stopped. These observations provide strong evidence that the initial shish growth occurs in discrete steps by the aggregation of pointlike nuclei into oriented threads.

The two nucleating particles, needlelike sodium benzoate (SB) and isotropic bicyclo[2.2.1]heptane-2,3-dicarboxylic acid (HPN), had different nucleation efficiencies with HPN having almost twice the nucleation efficiency of SB when compared at a similar particle surface area.

The addition of both nucleating particles increased the initial relaxation rate of shish after shear flow stopped. This result was explained by the presence of the particles inducing lower molecular weight chains to participate in shish formation. The lower molecular weight chains then destabilized the shish, accelerating their dissolution.

The addition of both nucleating particles resulted in a significant increase in the amount of shish and their size (length and diameter) compared to iPP(control). Possible mechanisms that could account for the particle-assisted formation of shish were discussed. The most likely mechanisms were based on the particles modifying the local strain environment near the particle surface.

The amount, dimensions, and alignment of the shish along the flow direction were much higher in iPP(1.00SB) compared to iPP(1.00HPN). These results imply that the shape of the nucleating particle can have important implications for the formation of shish. It was proposed that the needlelike SB particle adopted stable orientations along the flow direction, guiding shish growth, while isotropic HPN particles rotated during shear, destabilizing shish forming nearby.

## ■ AUTHOR INFORMATION

### Corresponding Author

\*E-mail andyphil21@gmail.com, Ph +613 9905 53213, Fax +613 9905 4940.

## ■ ACKNOWLEDGMENT

This work was performed at the SAXS/WAXS beamline at the Australian Synchrotron, Victoria, Australia. The assistance from Dr. Jan Ilavasky at Advanced Photon Source Argonne National Laboratory for modifying the Nika software package was greatly appreciated. The authors also acknowledge George Theodossiou at the Monash Centre for Electron Microscopy (MCEM) for preparing the SEM images.

## ■ REFERENCES

- (1) Keller, A.; Kolnaar, H. W. Flow induced orientation and structure formation. In *Materials Science and Technology, Processing of Polymers*; Meijer, H. E. H., Ed.; Wiley-VCH: New York, 1997; Vol. 18, p 189.
- (2) Janeschitz-Kriegl, H.; Ratajski, E. *Polymer* **2005**, *46*, 3856–3870.
- (3) Mykhaylyk, O. O.; Chambon, P.; Graham, R. S.; Fairclough, J. P. A.; Olmsted, P. D.; Ryan, A. J. *Macromolecules* **2008**, *41*, 1901–1904.
- (4) Mykhaylyk, O. O.; Chambon, P.; Impradice, C.; Fairclough, J. P. A.; Terrill, N. J.; Ryan, A. J. *Macromolecules* **2010**, *43*, 2389–2405.
- (5) Somani, R. H.; Yang, L.; Zhu, L.; Hsiao, B. S. *Polymer* **2005**, *46*, 8587–8623.
- (6) Hu, W.; Frenkel, D.; Mathot, V. B. F. *Macromolecules* **2002**, *35*, 7172–7174.
- (7) Housmans, J.-W.; Steenbakkers, R. J. A.; Roozemond, P. C.; Peters, G. W. M.; Meijer, H. E. H. *Macromolecules* **2009**, *42*, 5728–5740.
- (8) Kumaraswamy, G. *Polym. Rev.* **2005**, *45*, 375–397.
- (9) Fujiyama, M. Higher order structure of injection-moulded polypropylene. In *Polypropylene: Structure, Blends and Composites*; Karger-Kocsis, J., Ed.; Chapman & Hall: London, 1995; Vol. 1, pp 173–174.
- (10) Fujiyama, M.; Awaya, H.; Kimura, S. *J. Appl. Polym. Sci.* **1977**, *21*, 3291–3309.
- (11) Dukovski, I.; Muthukumar, M. *J. Chem. Phys.* **2003**, *118*, 6648–6655.
- (12) Pennings, A. J.; van der Mark, J. M. A. A.; Bouij, H. C. *Colloid Polym. Sci.* **1969**, *236*, 99–111.
- (13) Lieberwirth, I.; Loos, J.; Petermann, J.; Keller, A. *J. Polym. Sci., Part B: Polym. Phys.* **2000**, *38*, 1183–1187.
- (14) Kimata, S.; Sakurai, T.; Nozue, Y.; Kasahara, T.; Yamaguchi, N.; Karino, T.; Shibayama, M.; Kornfield, J. A. *Science* **2007**, *316*, 1014–1017.
- (15) Yamazaki, S.; Watanabe, K.; Okada, K.; Yamada, K.; Tagashira, K.; Toda, A.; Hikosaka, M. *Polymer* **2005**, *46*, 1685–1692.

- (16) Yamazaki, S.; Watanabe, K.; Okada, K.; Yamada, K.; Tagashira, K.; Toda, A.; Hikosaka, M. *Polymer* **2005**, *46*, 1675–1684.
- (17) Petermann, J.; Miles, M.; Gleiter, H. *J. Polym. Sci., Polym. Phys. Ed.* **1979**, *17*, 55–62.
- (18) Janeschitz-Kriegl, H.; Ratajski, E.; Stadlbauer, M. *Rheol. Acta* **2003**, *42*, 355–364.
- (19) Seki, M.; Thurman, D. W.; Oberhauser, J. P.; Kornfield, J. A. *Macromolecules* **2002**, *35*, 2583–2594.
- (20) Heeley, E. L.; Fernyhough, C. M.; Graham, R. S.; Olmsted, P. D.; Inkson, N. J.; Embrey, J.; Groves, D. J.; McLeish, T. C. B.; Morgan, A. C.; Meneau, F.; Bras, W.; Ryan, A. J. *Macromolecules* **2006**, *39*, 5058–5071.
- (21) Hoffman, J. D. *Polymer* **1979**, *20*, 1070–1077.
- (22) Clark, E. J.; Hoffman, J. D. *Int. J. Thermophys.* **1990**, *11*, 225–237.
- (23) Balzano, L.; Kukalyekar, N.; Rastogi, S.; Peters, G. W. M.; Chadwick, J. C. *Phys. Rev. Lett.* **2008**, *100*, 048302.
- (24) Keum, J. K.; Zuo, F.; Hsiao, B. S. *Macromolecules* **2008**, *41*, 4766–4776.
- (25) Patil, N.; Balzano, L.; Portale, G.; Rastogi, S. *Macromolecules* **2010**, *43*, 6749–6759.
- (26) Mathieu, C.; Thierry, A.; Wittmann, J. C.; Lotz, B. *J. Polym. Sci., Part B: Polym. Phys.* **2002**, *40*, 2504–2515.
- (27) Mathieu, C.; Thierry, A.; Wittmann, J. C.; Lotz, B. *Polymer* **2000**, *41*, 7241–7253.
- (28) D'Haese, M.; Van Puyvelde, P.; Langouche, F. *Macromolecules* **2010**, *43*, 2933–2941.
- (29) Zhu, P.; Phillips, A.; Edward, G.; Nichols, L. *Phys. Rev. E* **2009**, *80*, 051801.
- (30) Cacciuto, A.; Auer, S.; Frenkel, D. *Nature* **2004**, *428*, 404–406.
- (31) Chayen, N. E.; Saridakis, E.; Sear, R. P. *Proc. Natl. Acad. Sci. U.S.A.* **2006**, *103*, 597–601.
- (32) Somwangthanaroj, A.; Lee, E. C.; Solomon, M. J. *Macromolecules* **2003**, *36*, 2333–2342.
- (33) Rozanski, A.; Monasse, B.; Szkudlarek, E.; Pawlak, A.; Piorkowska, E.; Galeski, A.; Haudin, J. M. *Eur. Polym. J.* **2009**, *45*, 88–101.
- (34) Nowacki, R.; Monasse, B.; Piorkowska, E.; Galeski, A.; Haudin, J. M. *Polymer* **2004**, *45*, 4877–4892.
- (35) Jerschow, P.; Janeschitz-Kriegl, H. *Int. Polym. Process.* **1997**, *12*, 72–77.
- (36) Byelov, D.; Panine, P.; Remerie, K.; Biemond, E.; Alfonso, G. C.; de Jeu, W. H. *Polymer* **2008**, *49*, 3076–3083.
- (37) Huo, H.; Jiang, S.; An, L. *Macromolecules* **2004**, *37*, 2478–2483.
- (38) Zhu, P.; Tung, J.; Phillips, A.; Edward, G. *Macromolecules* **2006**, *39*, 1821–1831.
- (39) Zhu, P.; Phillips, A.; Tung, J.; Edward, G. *J. Appl. Phys.* **2005**, *97*, 104908.
- (40) Zhu, P.; Edward, G.; Nichols, L. *J. Phys. D: Appl. Phys.* **2009**, *42*, 245406.
- (41) Zhu, P.; Tung, J.; Edward, G.; Nichols, L. *J. Appl. Phys.* **2008**, *103*, 124906.
- (42) Phillips, A.; Zhu, P.; Edward, G. *Polymer* **2010**, *51*, 1599–1607.
- (43) Fu, B. X.; Yang, L.; Soman, R. H.; Zong, S. X.; Hsiao, B. S.; Phillips, S.; Blanski, R.; Ruth, P. *J. Polym. Sci., Part B: Polym. Phys.* **2001**, *39*, 2727–2739.
- (44) Mezghani, K.; Phillips, P. *J. Polymer* **1998**, *39*, 3735–3744.
- (45) Byelov, D.; Panine, P.; de Jeu, W. H. *Macromolecules* **2007**, *40*, 288–289.
- (46) Fillon, B.; Lotz, B.; Thierry, A.; Wittmann, J. C. *J. Polym. Sci., Part B: Polym. Phys.* **1993**, *31*, 1395–1405.
- (47) Fillon, B.; Wittmann, J. C.; Lotz, B.; Thierry, A. *J. Polym. Sci., Part B: Polym. Phys.* **2003**, *31*, 1383–1393.
- (48) Libster, D.; Aserin, A.; Garti, N. *Polym. Adv. Technol.* **2007**, *18*, 685–695.
- (49) Guinier, A. *Small-Angle Scattering of X-rays*; Wiley: New York, 1955.
- (50) Perret, R.; Ruland, W. *J. Appl. Crystallogr.* **1969**, *2*, 209–218.
- (51) Lotz, B.; Wittmann, J. C. *Polymer* **1996**, *37*, 4979–4992.
- (52) Turner-Jones, A. *Polymer* **1971**, *12*, 487–508.
- (53) De Rosa, C.; Auriemma, F.; Paolillo, M.; Resconi, L.; Camurati, I. *Macromolecules* **2005**, *38*, 9143–9154.
- (54) Keller, A.; MacKley, M. R. *Pure Appl. Chem.* **1974**, *39*, 195–224.
- (55) de Gennes, P. G. *J. Chem. Phys.* **1974**, *60*, 5030–5042.
- (56) Pennings, A. J.; Kiel, A. M. *Kolloid Z. Z. Polym.* **1965**, *205*, 160–162.
- (57) Janeschitz-Kriegl, H.; Ratajski, E.; Wippel, H. *Colloid Polym. Sci.* **1999**, *277*, 217–226.
- (58) Soman, R. H.; Yang, L.; Hsiao, B. S.; Agarwal, P. K.; Fruitwala, H. A.; Tsou, A. H. *Macromolecules* **2002**, *35*, 9096–9104.
- (59) Doi, M.; Edwards, S. F. *The Theory of Polymer Dynamics*; Clarendon Press: Oxford, 1986.
- (60) Vega, J. F.; Rastogi, S.; Peters, G. W. M.; Meijer, H. E. H. *J. Rheol.* **2004**, *48*, 663–678.
- (61) Garcia-Gutierrez, M.; Milner, S. T.; McLeish, T. C.; Hernandez, J. J.; Nogales, A.; Panine, P.; Rueda, D. R.; Ezquerra, T. A. *Macromolecules* **2007**, *41*, 844–851.
- (62) Kelarakis, A.; Yoon, K.; Sics, I.; Soman, R. H.; Chen, X.; Hsiao, B. S.; Chu, B. *J. Macromol. Sci., Part B: Polym. Phys.* **2006**, *45*, 247–261.
- (63) Soman, R. H.; Yang, L.; Hsiao, B. S. *Polymer* **2006**, *47*, 5657–5668.
- (64) Olmsted, P. D.; Poon, W. C. K.; McLeish, T. C. B.; Terrill, N. J.; Ryan, A. J. *Phys. Rev. Lett.* **1998**, *81*, 373–376.
- (65) Hwang, W. R.; Peters, G. W. M.; Hulsen, M. A.; Meijer, H. E. H. *Macromolecules* **2006**, *39*, 8389–8398.
- (66) Harlen, O. G.; Koch, D. L. *J. Fluid Mech.* **1993**, *252*, 187–207.
- (67) Jeffery, G. B. *Proc. R. Soc. London, Ser. A* **1922**, *102*, 161–179.
- (68) Gunes, D. Z.; Scirocco, R.; Mewis, J.; Vermant, J. *J. Non-Newtonian Fluid Mech.* **2008**, *155*, 39–50.
- (69) Hobbie, E. K.; Wang, H.; Kim, H.; Lin-Gibson, S.; Grulke, E. A. *Phys. Fluids* **2003**, *15*, 1196.
- (70) Hinch, E. J.; Leal, L. G. *J. Fluid Mech.* **1972**, *52*, 683–712.